

FATE: Focal-modulated Attention Encoder for Temperature Prediction

Tajamul Ashraf^{1, 2}, Janibul Bashir³

¹Indian Institute of Technology Delhi, India

²Microsoft Research, Bangalore, India

³National Institute of Technology Srinagar, India

tajamul@sit.iitd.ac.in, t-tashraf@microsoft.com, janibbashir@nitsri.ac.in

Code — <https://github.com/Tajamul21/FATE>

Abstract

One of the biggest issues facing humanity in the twenty-first century is climate change, as shown by the increasing sea levels, melting glaciers, and frequent storms. Accurate temperature forecasting is crucial for understanding and mitigating its impacts. Cutting-edge data-driven models for temperature forecasting typically employ recurrent neural networks (CNNs), with certain models integrating attention mechanisms. However RNNs sequential processing limits parallelization, especially for longer sequences. In order to do this, we provide a brand-new method for temperature prediction that is based on the FocalNet Transformer architecture. By functioning in a multi-tensor format, the suggested Focal-modulation Attention Encoder (FATE) framework leverages the spatial and temporal nuances of meteorological data characteristics by integrating tensorized modulation. Comparative assessments against existing transformer encoder architectures, 3D CNNs, LSTM, and ConvLSTM demonstrate our model's superior ability to capture nuanced patterns inherent in the data, particularly in the context of temperature prediction. We also introduce a new labeled dataset, Climate change Parameter dataset (CCPD), which encompasses 40 years of data from J&K region on seven key parameters that influence climate change, supporting further research in this area. Experiments on two real-world benchmark temperature datasets from weather stations in the USA, Canada, and Europe demonstrate accuracy improvements of 12%, 23%, and 28% respectively, compared to existing SOTA models. In addition, we achieved state-of-the-art results on our CCPD dataset with a 24% improvement. To understand FATE, we introduce two modulation scores from the tensorial modulation process. These scores clarify our model's decision-making and key climate change parameters. For reproducible research, we will release the source code, pre-trained FATE model, and CCPD dataset.

Introduction

The long-term transitions in climate parameter patterns, including temperature, precipitation, wind, and multiple facets related to the earth's climate, constitute climate change (Barrett, Charles, and Temte 2015). Climate change has drastic effects worldwide and may negatively affect life sustainability on the earth's surface. For instance, climate change may increase the earth's average temperature by 2°C in

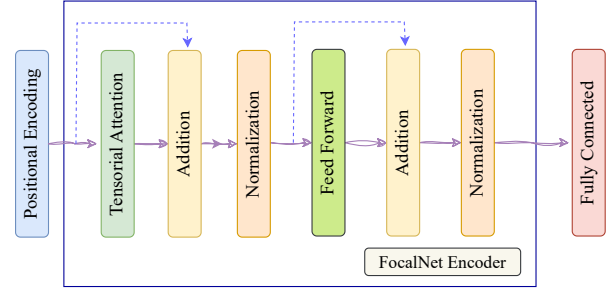


Figure 1: Model Architecture for Focal-modulated Tensorized Encoder (FATE) framework.

the current century, resulting in reduced crop yields. Climate change is a prolonged process and occurs over decades or longer. It mainly occurs due to the significant emission of Green House Gases (GHG), increased concentration of carbon dioxide due to the excessive fossil fuel burning and significant deforestation, and renewable energy generation (Latake, Pawar, and Ranveer 2015). Recently, policy-makers have made many efforts to control climate change by limiting the factors that significantly contribute to this change (Dunlap and McCright 2015). One promising step in this direction is the inclusion of Artificial Intelligence (AI) in understanding the factors responsible and determining the long-term effect of reactive strategies in combating climate change (Huntingford et al. 2019). The domain of AI makes it possible to analyze the enormous amount of data collected over the years and understand the patterns so that future trends can be forecasted well before (Hassani, Huang, and Silva 2019).

Reliable weather forecasts are essential for disaster management, economic sectors, and optimizing renewable energy. Accurate predictions of temperature and wind can greatly enhance energy generation and distribution efficiency. Domains spanning physics, computational science, and advanced machine learning frequently grapple with data that is structured in multi-dimensional formats. In the specific context of temperature applications, multi-dimensional tensor data encompasses diverse climate parameter variables measured across various time and spatial dimensions. Simply converting data into tensors may result in the loss of

valuable structural information. Moreover, exploring higher-order correlations, which involve relationships between different dimensions of the data, requires simultaneous consideration of all dimensions. As a result, tensorial machine learning models have garnered significant attention in recent years (Dai and Yeung 2006; Nguyen et al. 2015) for the analysis of high-dimensional data.

This paper introduces *FATE*, a tensor-based FocalNet Transformer model to preserve the spatial-temporal structure of climate data and effectively map inputs to outputs. It features a novel tensored modulation mechanism that improves model interpretability by analyzing modulation weights to assess the impact of climate parameters on temperature predictions. The study focuses on Jammu and Kashmir (J&K), where climate change has led to erratic snowfall and significant glacier retreat, with around 18% loss of Kolhai Glacier and 16% in the Suru Basin over the past forty years (Kumar et al. 2013; Hassan 2014). The AI tool developed aims to analyze these trends and predict long-term climate impacts.

Contributions of this work:

- We developed an innovative transformer architecture that incorporates a new focal-modulation mechanism specifically designed to analyze data with 3D tensor format.
- We introduce two modulation scores from tensorial modulation, which enhance the model’s ability to capture key aspects of 3D tensor data and improve performance on complex structures.
- To evaluate the proposed *FATE* model, we compare it against classical models, including the encoder transformer, 3D CNN, LSTM, and Convolutional LSTM, on the temperature prediction task.
- We introduce a new comprehensive dataset (CCPD) spanning over 40 years, with a specific focus on the Pir Panjal range in Jammu and Kashmir.
- Using reference temperature datasets from US, Canadian, and European weather stations, we get a new SOTA with accuracy gains of 12%, 23%, and 28%, in that order. The proposed *FATE* model’s explainability has been improved by the application of data visualization tools.

Background and Related Work

Climate parameters and Temperature Forecasting

The changing climate, driven by global warming and human activities like greenhouse gas emissions, has led to drastic environmental changes. We reviewed recent advancements in artificial intelligence (AI) for climate change through cutting-edge technologies and research. In recent years, machine learning algorithms have seen substantial advancements, leading to breakthroughs across various domains, including climate analysis (Zhu et al. 2017). The emergence of data-driven models has notably reduced processing time for climate parameters forecasting (Trebing and Mehrkanoon 2020; Ravuri et al. 2021). These models rely on extensive historical climate observations to extract and comprehend intricate input-output mappings, subsequently enabling the

prediction of future climate conditions (Mehrkanoon 2019; Kuligowski and Barros 1998).

Despite these advancements, predicting climate parameters remains challenging due to the spatiotemporal characteristics of climate data and its intricate nonlinear behavior (Bartos and Jánosi 2006). With the increasing availability of climate data and the continuous improvement of computing power, researchers are actively exploring diverse data-driven models. Artificial Neural Networks (ANN) (Salman, Kanigoro, and Heryadi 2015) have proven effective, with CNNs and RNNs, including Long Short-Term Memory (LSTM) networks, demonstrating precise prediction of hourly air temperature, particularly for individual time steps into the future (Soman et al. 2010; Cifuentes et al. 2020). CNN-based models, devoid of the need for explicit feature engineering, rely on automatic feature extraction during network training (Kreuzer, Munz, and Schlüter 2020). For instance, in temperature forecasting, Mehrkanoon (Mehrkanoon 2019) proposed a 3D-Convolutional model, while Klein et al. (Klein, Wolf, and Afek 2015) introduced the Innovative Convolutional Layer with a dynamic update mechanism, a novel approach for short-range climate prediction tasks where filters dynamically change with inputs during testing.

Modeling long-term dependencies in time-series data is a strong suit for Recurrent Neural Networks (RNNs) (Kreuzer, Munz, and Schlüter 2020), especially LSTM networks (Hochreiter and Schmidhuber 1997). Combining CNN and RNN, the Long- and Short-term Time-series Network (LSTNet) (Lai et al. 2018) detects long-term patterns in time series data and captures short-term local dependencies. Furthermore, for precipitation prediction, the ConvLSTM network combines the CNN and LSTM architectures (Shi et al. 2015). However, because recurrent neural networks process information sequentially, their hierarchical processing makes simultaneous training difficult, particularly for large sequence lengths (Vaswani et al. 2017).

Geographic Information Systems (GIS) play a vital role in spatial data analysis, offering tools for visualization, organization, and analysis. ArcGIS, a leading GIS software by ESRI, facilitates tasks like map overlay and spatial data classification. Leveraging unsupervised learning in ArcGIS enhances applications such as environmental monitoring and disaster management (Malczewski 2004; Lloyd et al. 2020). Statistical measures like Pearson’s correlation coefficient are applied to examine relationships between variables, supporting spatial data analysis for informed decision-making. In this work, we utilize the Pearson correlation coefficient to analyze relationships between variables.

As data availability and deep learning techniques advance, improvements in temperature prediction accuracy are anticipated, benefiting fields such as agriculture and transportation (Livieris, Pintelas, and Pintelas 2020). Our study utilizes atmospheric variables to train LSTM and BiLSTM models, demonstrating the effectiveness of stacked LSTM models for temperature prediction (Karevan and Suykens 2018). We also incorporate an attention mechanism (Vaswani et al. 2017) with Recurrent Neural Networks to capture dependencies in long sequences. The Temporal Pattern Attention LSTM (TPA-LSTM) (Shih, Sun, and Lee

2019) leverages this mechanism to focus on relevant past time steps and discern inter-dependencies among features.

Transformers

The Transformer model, an innovative attention-based architecture, was first introduced in 2017 (Vaswani et al. 2017). This architecture revolutionized the handling of sequential data by introducing the attention mechanism, which enables simultaneous processing of all input tokens. Unlike conventional encoder-decoder architectures that often employ recurrent layers for sequential processing, the Transformer replaces them with multi-headed self-attention. In the Transformer’s attention mechanism, dot-product attention incorporates an amplifying coefficient based on the key dimension (Vaswani et al. 2017).

By releasing the model from the confines of sequential data processing, this design decision offers potential for parallelization and shortens training durations computationally (Vaswani et al. 2017). Furthermore, the additive attention mechanism is a frequently employed substitute attention mechanism that computes attention weights via a feed-forward neural network (Bahdanau, Cho, and Bengio 2014). Recent years have seen tremendous progress in sequence-to-sequence model development, with the Transformer architecture emerging as a key instrument in natural language processing. Machine translation (Vaswani et al. 2017), document generation (Liu et al. 2018), and syntactic parsing (Kitaev and Klein 2018) are only a few of the tasks that this architecture has significantly improved.

Focal modulation networks (Focalnet) by Jainwei et al. (Yang et al. 2022) provide a paradigm shift by entirely replacing self-attention (SA) with a focal modulation module for robust token interaction modeling. The focal modulation comprises focal contextualization, gated aggregation, and element-wise affine transformation (Yang et al. 2022). Building on that, TransFED (Ashraf, Bin Afzal Mir, and Gillani 2024) introduced an innovative learn-to-tailor approach, mitigating the detrimental effects of FedAvg on focal modulation and achieving superior performance in scenarios with heterogeneous data distributions. Multi-mask Tensorized Self Attention (MSTA) by Shen et al. (Shen et al. 2018) introduces an innovative approach, capturing dependencies between token pairs through amplified dot-product attention. This method is based on a multi-dimensional attention mechanism to calculate token contributions across various feature dimensions for a given NLP task. The Informer architecture, as presented by Zhou et al. (Zhou et al. 2021), boasts the ProbSparse attention mechanism, adept at efficiently handling extremely long sequences. This mechanism generates limited key-query pairs for each attention head, mitigating loss. Similarly, Ma et al. (Ma et al. 2019) contribute to the field by leveraging a tensorized transformer to compress model parameters effectively using Tucker decomposition (Tucker 1966) in a self-attention block, reconstructing amplified dot-product attention.

This paper presents the Focal Modulated Tensorized Encoder (FATE) framework designed for the temperature forecasting task. The model features a novel tensorized modulation mechanism. In contrast to (Ma et al. 2019), our novel

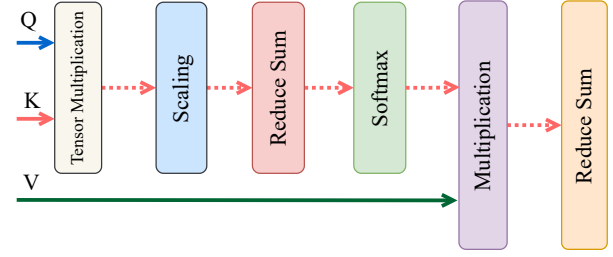


Figure 2: Tensorial Focal Modulation

FATE framework accepts input in the form of 3D tensors and preserves this tensor format throughout the entire focal modulation layer computation. FATE, facilitated by the introduced tensorized focal modulation mechanism, adeptly captures long-range correlations between time stamps and climate change parameters by attending to all dimensions of the data simultaneously. Detailed explanations of our proposed model will follow in the subsequent sections.

Proposed Methodology

Multi-Dimensional Tensorized FocalNet Encoder

In this study, we expand upon the foundational Focalnet Transformer (Yang et al. 2022) and present the Tensorized Focal Encoder Transformer framework, tailored for discerning intricate patterns within multi-dimensional input data. More precisely, our model operates on climate change parameter inputs structured in a 3D tensorial format $X \in \mathbb{R}^{T \times S \times P}$, where T denotes the number of time steps, and S and P characterize the dimensions corresponding to 2D features.

The 2D features, represented as $S \times P$, constitute a matrix that captures diverse climate parameters such as temperature, humidity, wind speed, etc. Specifically, different stations are arranged along dimension S , while the various climate parameters are distributed along dimension P . The proposed architecture takes the form of an encoder-only Transformer architecture, as depicted in Fig. 1. It encompasses a layer with positional encoding, an encoder layer, and a linear activated fully-connected layer. The encoder layer integrates tensorial modulation, details of which will be presented in Sections 3.2 and 3.3. Following tensorial modulation, there exists a residual connection and a normalization layer. In this framework, a densely connected FFN incorporating two linear transformations and Rectified Linear Unit (ReLU) activation follows the tensorial focal modulation layer. Consistent with (Yang et al. 2022), this is succeeded by an additional residual connection and normalization layer.

Tensorial Focal Modulation

We utilize a constant positional encoding to integrate temporal hierarchical information into the model. The positional encoding, as described in (Yang et al. 2022), is computed for the time step T and parameter P according to Eq (1),

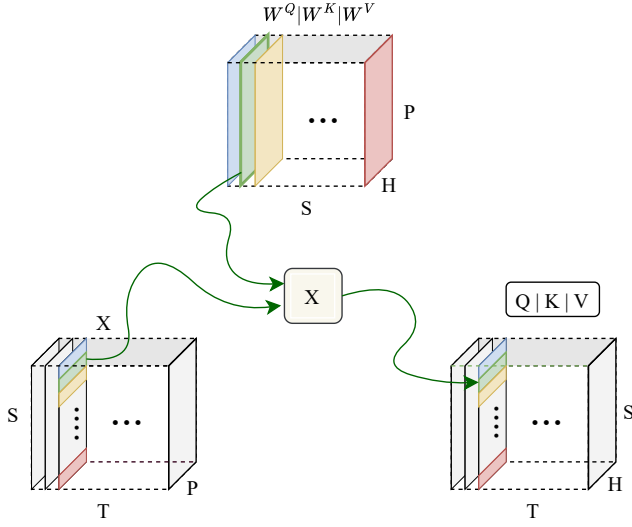


Figure 3: The image illustrates how slice multiplication with weight tensors extracts query (Q), key (K), and value (V) tensors from an input tensor (X). Each color represents a vector slice in X , which is multiplied by matching-colored matrix slices of weights, producing corresponding vector slices in the output tensors Q , K , and V .

$$\text{PE}(\text{pos}, 2i) = \sin\left(\frac{\text{pos}}{10000 \cdot 2^i / P}\right) \quad (1)$$

where the location along the parameter axis is represented by i and the position along the time axis by pos . The station axis S is used to transmit the resultant values.

We employ the following terminology to define tensorial focused modulation (see Fig. 2). The matrix $(N_{y,z})_x \in \mathbb{R}^{Y \times Z}$, which consists of all values of the tensor N when the first dimension is set to x , represents the x -slice for a tensor $N \in \mathbb{R}^{X \times Y \times Z}$. The tensor $(N_z)_{x,y} \in \mathbb{R}^Z$, which consists of the values of N with the first and second dimensions set to x and y , respectively, is used to represent the x, y -slice of N . The lowercase letter that corresponds to the particular dimension indicates the size of the slice.

The tensorial focal modulation takes a 3D tensor as input $X \in \mathbb{R}^{T \times S \times P}$. In the initial phase of tensorial focal modulation, distinct 3D Query (Q), Key (K), and Value (V) tensors are computed, each with dimensions $\mathbb{R}^{T \times S \times H}$. This computation involves element-wise multiplication between the input tensor X and three separate weight tensors, namely W_Q , W_K , and W_V , each with dimensions $\mathbb{R}^{S \times F \times H}$. The t, s slice of Q , K , and V (denoted as $(Q_h)_{t,s}$, $(K_h)_{t,s}$, and $(V_h)_{t,s}$ respectively) is computed by element-wise multiplication between the t, s slice of X (denoted as $(X_p)_{t,s}$) and the s slice of W^Q , W^K , and W^V (represented as $(W^Q)_{p,h,s}$, $(W^K)_{p,h,s}$, and $(W^V)_{p,h,s}$ respectively), following the expressions:

$$\begin{aligned} (Q_h)_{t,s} &= (X_p)_{t,s} \times (W^Q)_{p,h,s}, \quad \forall t = 1..T, s = 1..S, \\ (K_h)_{t,s} &= (X_p)_{t,s} \times (W^K)_{p,h,s}, \quad \forall t = 1..T, s = 1..S, \\ (V_h)_{t,s} &= (X_p)_{t,s} \times (W^V)_{p,h,s}, \quad \forall t = 1..T, s = 1..S. \end{aligned} \quad (2)$$

Figure 3 displays the depiction of the multiplication operations given in Eq (2). The subsequent step involves computing the product of every time step t slice of Q (referred to as $(Q_{s,h})_t$) and the transpose of every time step t^l slice of K (referred to as $((K_{s^l,h})_{t^l})^T$). These multiplicative operations provide matrices $(\tilde{R}_{s,s^l})_{t,t^l}$ with dimensions $S \times S^l$, as given by eq (3) and eq (4). Together, these matrices make up slices of a tensor $\tilde{R} \in \mathbb{R}^{T \times T^l \times S \times S^l}$, where the first and second dimensions of the Q tensor are denoted by T and S respectively, while the initial and secondary dimensions of the K tensor are indicated by T^l and S^l .

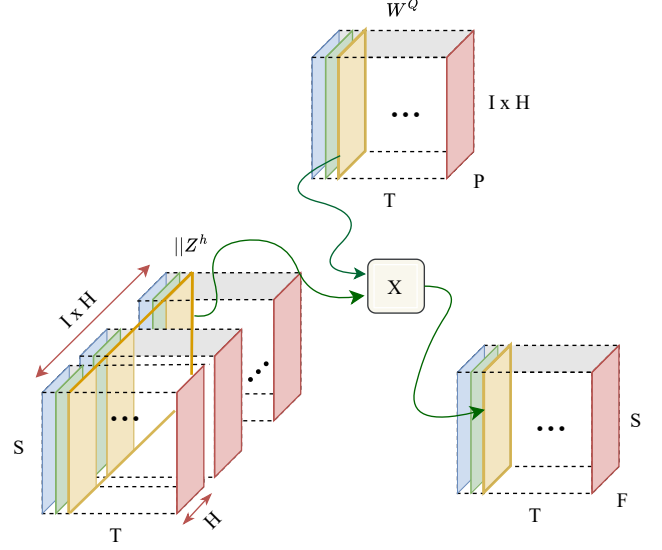


Figure 4: The illustration demonstrates the slice multiplication process used to derive the multi-head attention output Y from the concatenated self-attention output tensors. Each color in the figure corresponds to time slices in the concatenated self-attention tensors, which are multiplied by the corresponding time slices of the weight tensor. This operation results in the formation of a time slice of the same color in the output tensor Y .

Following the methodology outlined in Vaswani et al.'s work (Vaswani et al. 2017), the tensor \tilde{R} undergoes summation along its last dimension, followed by an element-wise division by the square root of H . This process results in tensor $R \in \mathbb{R}^{T \times T^l \times S}$.

$$\begin{aligned} (\tilde{R}_{s,h^l})_{t,t^l} &= (Q_{s,h})_t \times ((K_{s^l,h})_{t^l})^T, \quad \forall t, t^l = 1, \dots, T, \\ R &= \frac{1}{\sqrt{H}} \sum_{s^l=1}^S (\tilde{R}_{t,t^l,s})_{s^l}. \end{aligned} \quad (3)$$

Subsequently, a softmax operation is applied to each t, t^l slice of R across its final dimension S to produce attention weights $\tilde{A} \in \mathbb{R}^{T \times T^l \times S}$, as depicted in eq (4).

$$(\tilde{A}_s)_{t,t^l} = \text{Softmax}((R_{t,t^l,s})_s), \quad \forall t, t^l = 1, \dots, T. \quad (4)$$

Subsequent to applying softmax, the attention weights \tilde{A} undergo multiplication by the transpose of the time slice t^l of V , represented by $(V_{t^l})_{s^l}$ in eq (5), resulting in the generation of self-attention tensor $A \in \mathbb{R}^{T \times S \times H}$.

$$(A_h)_{t,s} = (\tilde{A}_s)_{t,t^l} \times (V_h)_{t^l,s}, \quad \forall t, t^l = 1, \dots, T. \quad (5)$$

Finally, as depicted in eq (6) and Fig. 4, a fully connected layer combines all the self-attention heads $A^h \in \mathbb{R}^{T \times S \times H}$ to produce the final output $Y \in \mathbb{R}^{T \times S \times P}$.

$$(Y_h)_{t,s} = \sum_{h=1}^H (A_h)_{t,s} \times (W^O)_{h,p}. \quad (6)$$

The resulting Y tensor is passed through a normalization layer and a residual connection before being fed into the next layer of the transformer encoder. This completes the process of tensorial focal modulation in our proposed architecture.

Experiments

Using the three benchmark datasets shown in Table 1, we implement our proposed Focal-modulated Tensorized Encoder (FATE) framework and compare the results with four alternative models: the conventional encoder Transformer (Vaswani et al. 2017; Yang et al. 2022) (with the flattened input tensor), 3D-CNN (Mehrkanoon 2019), LSTM (Hochreiter and Schmidhuber 1997), and Conv LSTM (Shi et al. 2015). As per the methods described in (Mehrkanoon 2019), we use the Mean Absolute Error (MAE) and Mean Squared Error (MSE) metrics to evaluate the effectiveness of the models. These may be explained as follows:

$$\text{MAE} = \frac{\sum_{i=1}^n |y_i - \hat{y}_i|}{n}, \quad \text{MSE} = \frac{\sum_{i=1}^n (y_i - \hat{y}_i)^2}{n}, \quad (7)$$

where N represents the no. of samples, y_i is the actual sur-

Dataset	Dataset Size			Details	
	Train	Validation	Test	Cities	Features
CCPD (In house)	4500	365	1235	3	6
USA-Canada	35362	1024	7997	30	11
Europe	3854	512	1086	18	19

Table 1: Dataset Statistics

face temperature value, and \hat{y}_i is the predicted surface temperature value. The training procedure encompasses the application of the MSE loss function for up to 100 epochs, with early termination determined by the validation loss. The Adam optimizer (Kingma and Ba 2014) is employed

across all models. While FATE and Transformer incorporate a tailored learning rate schedule (Vaswani et al. 2017), 3D-CNN, LSTM, and Conv LSTM dynamically adjust their learning rates using the Adam optimizer. The optimized hyperparameters for each model are detailed in Table 2.

Hyper-parameter	FATE	Transformer	3D CNN	LSTM	ConvLSTM
Focal Levels	4	3	-	-	-
Layer Number	1	1	-	1	3
Head	8	1	-	-	-
Key Dim	32	32	-	-	-
Dense Units	64	64	128	-	-
Filters	-	-	10	-	16
Kernel Size	-	-	4	-	13
Hidden Units	-	-	-	128	-
Learning Rate	Schedule	Schedule	10^{-4}	10^{-4}	10^{-4}
Batch Size	64	32	128	256	128

Table 2: Hyper-parameters used for all the models

CCPD (In House) Dataset

Data Collection The assessment was conducted using the following seven parameters: *Air Index*, *Forest Cover*, *Water Bodies*, *Agriculture and Vegetation*, *Population*, *Surface Temperature*, and *Construction*. For the purposes of assessing forest cover, agriculture, and water bodies, satellite data from Landsat TM (1960, 2011), Landsat MSS (1980), Landsat ETM (1992), and Landsat ETM+ (2001, 2009) were used. This allowed for a 12-month data set acquired across four decades, with a three to five-day interval between selected dates.

The spatial resolution of 30m and spectral wavelength of seven bands facilitated detailed analysis. ESRI ArcMap 10.8 and Pandas/NumPy libraries were employed for spatial and data analysis. Sub-pixel level accuracy enhanced precision, and image processing techniques were applied, including contrast stretching, histogram adjustments, filtering, and band variations. Local focus on the Region of Interest (ROI) facilitated maximum information extraction, boundary identification between classes, and effective classification. The rigorous data collection process ensures a comprehensive understanding of climate change factors in the region.

For Population Data, census data collected by the Ministry of Home Affairs was utilized. The population of Jammu and Kashmir grew from 2,139,362 in 1901 to 12.5 million in 2011. based on Sumira et al.’s 2013 study, surface temperature data revealed a 1.2°C increase in the ROI from 1980 to 2010 (Zaz and Romshoo 2013). Construction areas were analyzed using Google Earth and K-means Clustering to identify changes over time. Air Index data, sourced from UrbanEmissions (Gani et al. 2022), which utilized satellite data and chemical transport models to obtain PM2.5 concentrations (Mandal et al. 2020; Weagle et al. 2018). The data correlations, detailed in Table 3, were analyzed following the Data Collection phase. Most parameters exhibit positive correlations. However, forest cover is an exception, displaying

Variable	Population	Forest Cover	Temperature	Water Bodies	Construction	Agriculture	Air Index
Population	1.000	-0.960	0.870	0.854	0.922	0.943	0.743
Forest Cover	-0.960	1.000	-0.767	-0.780	-0.986	-0.963	-0.834
Temperature	0.870	-0.767	1.000	0.765	0.692	0.698	0.522
Water Bodies	0.854	-0.780	0.765	1.000	0.724	0.775	0.369
Construction	0.922	-0.986	0.692	0.724	1.000	0.978	0.893
Agriculture	0.943	-0.963	0.698	0.775	0.978	1.000	0.861
Air Index	0.743	-0.834	0.522	0.369	0.893	0.861	1.000

Table 3: Correlation Table between various parameters.

a negative correlation. This negative correlation is attributed to the gradual reduction in forest cover over time.

Results. For this dataset, experiments were conducted to make predictions for 2, 4, and 6 weeks into the future. The regressor was constructed using an empirically determined optimal lag parameter of 5 weeks. The focus was on predicting surface temperature, which served as both the target parameter and feature. Table 4 summarizes the MAE and MSE results from these experiments. The proposed FATE model consistently demonstrates superior performance compared to other models, particularly excelling in forecasting surface temperature for 3 and 6 weeks ahead.

Station	Model	MAE			MSE		
		2 weeks	4 weeks	6 weeks	2 weeks	4 weeks	6 weeks
Rajori	Transformer	3.859	4.055	4.788	8.623	9.263	12.653
	3D CNN	3.981	4.523	4.898	9.734	10.684	12.704
	LSTM	4.366	4.801	4.931	9.354	13.282	15.884
	ConvLSTM	5.159	5.787	5.948	11.82	11.525	14.265
	FATE	3.068	3.542	3.848	5.133	8.719	10.144
Poonch	Transformer	5.823	5.992	6.452	5.841	6.163	8.636
	3D CNN	5.963	5.125	6.465	6.215	6.251	9.854
	LSTM	5.941	6.225	6.521	6.362	6.325	8.921
	ConvLSTM	6.201	6.142	6.784	6.621	6.854	12.563
	FATE	5.652	5.982	6.234	5.879	6.023	6.365
Ramban	Transformer	4.432	4.871	5.688	6.021	6.325	7.652
	3D CNN	4.751	4.987	5.854	6.329	6.641	8.519
	LSTM	4.450	5.211	6.218	6.398	6.823	9.175
	ConvLSTM	5.317	5.638	7.622	6.821	8.744	11.368
	FATE	4.215	4.598	5.142	5.871	5.924	8.145

Table 4: MAE and MSE for each model at different time horizons for Rajori, Poonch, and Ramban stations for CCPD dataset.

USA-Canada Dataset

The **USA-Canada** dataset encompasses hourly recordings of diverse weather parameters, such as air pressure, humidity, surface temperature, wind direction, and wind speed. Collected from October 2012 to November 2017, the observations cover 30 cities in the USA and Canada. The geographical coordinates of these cities are converted into Cartesian coordinates, and these normalized coordinates are included as three additional features in the dataset.

$$x = \cos(\phi) \cdot \cos(\lambda), \quad (8)$$

$$y = \cos(\phi) \cdot \sin(\lambda), \quad (9)$$

$$z = \sin(\phi). \quad (10)$$

where the latitude and longitude are indicated by ϕ and λ , respectively. Each sample is enhanced with the day of the year and the hour of the day in order to address temporal periodicity within the data. Both the measurements and this enhanced feature set are scaled, as shown in Eq. (11). The

Station	Model	MAE				MSE			
		4 hrs	8 hrs	12 hrs	16 hrs	4 hrs	8 hrs	12 hrs	16 hrs
Vancouver	Transformer	1.238	1.858	1.987	2.146	2.566	5.787	6.617	7.748
	3D CNN	1.499	1.896	2.131	2.329	3.704	5.950	7.455	8.879
	LSTM	1.311	1.834	2.039	2.210	2.917	5.712	6.970	8.237
	ConvLSTM	1.338	1.829	1.992	2.194	2.967	5.553	6.571	7.990
	FATE	1.021	1.217	1.346	1.131	1.464	1.660	1.844	2.238
New York	Transformer	1.426	2.043	2.271	2.489	3.836	7.533	9.268	10.978
	3D CNN	1.835	2.316	2.833	2.673	5.587	9.159	13.468	11.964
	LSTM	1.596	2.126	2.325	2.507	4.724	8.103	9.749	10.985
	ConvLSTM	1.394	2.134	2.419	2.104	4.949	7.790	9.257	10.341
	FATE	1.298	1.689	1.974	1.995	3.180	5.296	6.677	8.193
Los Angeles	Transformer	1.426	2.043	2.271	2.489	3.836	7.533	9.268	10.978
	3D CNN	1.835	2.316	2.833	2.673	5.587	9.159	13.467	11.968
	LSTM	1.296	2.026	2.325	2.207	4.724	8.403	9.749	10.983
	ConvLSTM	1.594	2.134	2.419	2.704	4.949	7.790	8.457	12.342
	FATE	1.183	1.530	1.920	2.041	3.180	5.496	6.677	8.185

Table 5: Mean Absolute Error (MAE) and Mean Squared Error (MSE) for surface temperature prediction on the **USA-Canada** dataset.

data from 2016 to 2017 makes up the test set, and the dataset from 2012 to 2016 makes up the train and val set.

$$x_{\text{scaled}} = \frac{x - \min(x)}{\max(x) - \min(x)}. \quad (11)$$

The time sequence, cities, and city characteristics are represented by a tensor of dimensions $T \times C \times F$, which we use to represent the input data. Future time steps—that is, 2, 6, 8, and 21 hours ahead of time—are predicted.

In this dataset, Vancouver, Dallas, and New York are identified as the target cities, and surface temperature is selected as the target feature. The results for MAE and MSE on the test set are presented in Table 5. Notably, the prediction accuracy shows a decrease as the forecasting horizon increases. Across all tested time steps ahead, our proposed FATE model consistently outperforms the other models, exhibiting the minimum MAE and MSE over all three cities and prediction times.

Europe Dataset

This dataset includes daily weather observations for eighteen European cities from May 2005 to April 2020. The day of the year is added and normalized together with other parameters in order to represent temporal periodicity. The test set is from 2017 to 2020, while the training and validation period is from 2005 to 2017.

This dataset’s experiments concentrate on forecasting surface temperatures three, five, and seven days in advance. The ideal lag parameter for building regressors is found through empirical research, and it is fixed at six days. The average surface temperature is the aim characteristic, and the target cities are Munich, Maastricht, and Barcelona. Table 7 presents MAE and MSE. The suggested fate model performs the second-best overall. When it comes to forecasting Maastricht’s surface temperature for the next five and seven days, it beats other models handily. With the greatest MAE in five prediction tasks and the best MSE in four, LSTM is clearly the highest-performing model in this dataset. (Guo et al. 2019) and (Ezen-Can 2020) have previously proposed that Transformers may have issues with tiny datasets.

Variable	Modulation Score (2 weeks)	Variable	Modulation Score (4 weeks)	Variable	Modulation Score (6 weeks)	Variable	Modulation Score (8 weeks)
F_c	0.34	F_c	0.31	F_c	0.35	F_c	0.28
P	0.12	P	0.12	P	0.19	P	0.12
W_b	0.05	W_b	0.23	W_b	0.01	W_b	0.13
C	0.26	C	0.26	C	0.25	C	0.21
A_g	0.21	A_g	0.06	A_g	0.09	A_g	0.14
A_I	0.02	A_I	0.08	A_I	0.11	A_I	0.12

Table 6: Modulation scores over different time periods. In the table, T : surface temperature, t : time, F_c : Forest Cover, W_b : Water Bodies, C : Construction, A_g : Agriculture, and A_I : Air Index. The modulation score of the parameter represents the amount of modulation each of the heads is paying to the parameters. The modulation score indicates the importance of each parameter in the temperature prediction.

Station	Model	MAE			MSE		
		3 days	5 days	7 days	3 days	5 days	7 days
Barcelona	Transformer	2.608	2.901	3.347	11.702	14.660	15.926
	3D CNN	2.502	3.015	3.059	10.73	13.654	15.740
	LSTM	2.303	2.801	2.931	9.354	11.328	14.931
	ConvLSTM	2.759	2.787	2.948	12.882	12.272	14.920
	FATE	2.474	2.665	2.995	9.415	11.094	13.523
Maastricht	Transformer	4.770	5.293	5.649	30.891	43.283	50.678
	3D CNN	4.276	5.078	5.609	28.823	40.531	49.410
	LSTM	3.982	5.036	5.373	24.860	39.484	46.590
	ConvLSTM	4.578	4.863	5.322	32.699	39.819	43.288
	FATE	4.164	4.910	4.940	26.458	35.501	39.707
Munich	Transformer	4.136	5.286	5.275	23.954	39.057	43.526
	3D CNN	3.931	5.049	5.262	24.870	39.578	43.507
	LSTM	3.551	4.730	5.189	20.235	34.021	42.733
	ConvLSTM	3.974	4.830	5.023	22.484	35.401	37.767
	FATE	3.196	4.935	5.125	19.927	35.454	38.309

Table 7: MAE and MSE results for surface temperature prediction in the **Europe** dataset

Modulation Visualization and Ablation study

As shown for New York in Fig. 5 (a)–(d), the modulation scores NP_h^v from Eq (??) show the parameters to which each head concentrates while anticipating the model’s output. The contribution of each city to the target city is measured by computing AS_c from Eq (??). Figs. 5(e)–(h) provide attention visualizations for the target cities. Cities’ names and numbers are used to symbolize the heads in Tensorial multi-head attention in Fig. 5(a)–(d). The visualization shows how much each head pays attention to the connected city based on the thickness of the lines. Only the cities receiving the most attention are displayed, along with the matching heads, for improved clarity. The importance of each city in predicting the temperature of the target city is shown by circle sizes in Figures 5(e)–(h). The red circle that highlights the target city indicates how important it is to pay attention to itself. The target city is often further away from the most significant cities considered in the prediction as the forecast horizon grows.

In the ablation study, we evaluate six parameters: Forest Cover, Water Bodies, Agriculture and Vegetation, Population, Construction, and Air Index. To assess the effect of each parameter on surface temperature, we calculate NP^v as defined in Eq (??). Table 6 provides a summary of the predicted surface temperatures and modulation scores for these parameters across different weeks.

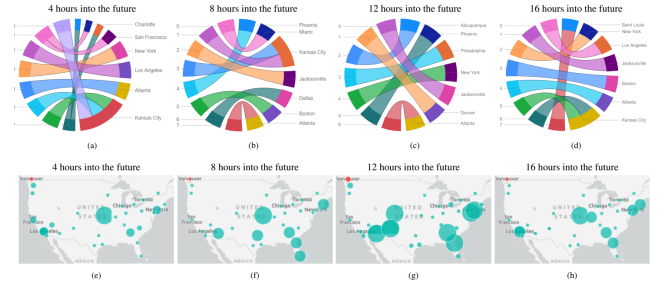


Figure 5: Modulation attention for New York in the **USA-Canada** dataset is visualized. Circular graphs show which cities each key head attends to, with line thickness indicating the level of attention. Circle sizes represent each city’s importance in predicting the target city’s temperature, with the target city highlighted in red.

Conclusion

In this study, we tackled the issue of increasing temperatures by proposing a new approach: the focal-modulated tensorized encoder (FATE) framework. This innovative framework effectively captures various factors contributing to climate change acceleration. Additionally, we offer a comprehensive climate dataset from the Pir Panjal range, covering the past 40 years. The performance of FATE is assessed on three real-world weather datasets, where it surpasses other models in the **Inhouse** and **Europe** datasets. For the **USA-Canada** dataset, our model generally performs the best. We introduce two modulation scores and conduct ablation studies to provide deeper insights into the model’s predictions. Our goal is to offer valuable insights to inform proactive climate policies and measures, and to enable applications with 3D tensor data.

Acknowledgements

This work was supported by the Jammu and Kashmir Science Technology and Innovation Council under Project no: JKST&IC/SRE/336-40. We express our deepest gratitude to the council for their invaluable support and funding, which were crucial for the successful completion of this research.

References

Ashraf, T.; Bin Afzal Mir, F.; and Gillani, I. A. 2024. TransFed: A Way To Epitomize Focal Modulation Using

- Transformer-Based Federated Learning. In *Proceedings of the IEEE/CVF Winter Conference on Applications of Computer Vision (WACV)*, 554–563.
- Bahdanau, D.; Cho, K.; and Bengio, Y. 2014. Neural machine translation by jointly learning to align and translate. *arXiv preprint arXiv:1409.0473*.
- Barrett, B.; Charles, J. W.; and Temte, J. L. 2015. Climate change, human health, and epidemiological transition. *Preventive medicine*, 70: 69–75.
- Bartos, I.; and Jánosi, I. 2006. Nonlinear correlations of daily temperature records over land. *Nonlinear Processes in Geophysics*, 13(5): 571–576.
- Cifuentes, J.; Marulanda, G.; Bello, A.; and Reneses, J. 2020. Air temperature forecasting using machine learning techniques: a review. *Energies*, 13(16): 4215.
- Dai, G.; and Yeung, D.-Y. 2006. Tensor embedding methods. In *AAAI*, volume 6, 330–335.
- Dunlap, R. E.; and McCright, A. M. 2015. Challenging climate change. *Climate change and society: Sociological perspectives*, 300.
- Ezen-Can, A. 2020. A Comparison of LSTM and BERT for Small Corpus. *arXiv preprint arXiv:2009.05451*.
- Gani, S.; Pant, P.; Sarkar, S.; Sharma, N.; Dey, S.; Guttikunda, S. K.; AchutaRao, K. M.; Nygard, J.; and Sagar, A. D. 2022. Systematizing the approach to air quality measurement and analysis in low and middle income countries. *Environmental Research Letters*, 17(2): 021004.
- Guo, Q.; Qiu, X.; Liu, P.; Shao, Y.; Xue, X.; and Zhang, Z. 2019. Star-transformer. *arXiv preprint arXiv:1902.09113*.
- Hassan, R. 2014. Disasters in Kashmir: Impact and Response. *Journal of Humanities and Social Science*, 19(7): 32–42.
- Hassani, H.; Huang, X.; and Silva, E. 2019. Big data and climate change. *Big Data and Cognitive Computing*, 3(1): 12.
- Hochreiter, S.; and Schmidhuber, J. 1997. Long short-term memory. *Neural computation*, 9(8): 1735–1780.
- Huntingford, C.; Jeffers, E. S.; Bonsall, M. B.; Christensen, H. M.; Lees, T.; and Yang, H. 2019. Machine learning and artificial intelligence to aid climate change research and preparedness. *Environmental Research Letters*, 14(12): 124007.
- Karevan, Z.; and Suykens, J. A. 2018. Spatio-temporal stacked LSTM for temperature prediction in weather forecasting. *arXiv preprint arXiv:1811.06341*.
- Kingma, D. P.; and Ba, J. 2014. Adam: A method for stochastic optimization. *arXiv preprint arXiv:1412.6980*.
- Kitaev, N.; and Klein, D. 2018. Constituency parsing with a self-attentive encoder. *arXiv preprint arXiv:1805.01052*.
- Klein, B.; Wolf, L.; and Afek, Y. 2015. A dynamic convolutional layer for short range weather prediction. In *Proceedings of the IEEE Conference on Computer Vision and Pattern Recognition*, 4840–4848.
- Kreuzer, D.; Munz, M.; and Schlüter, S. 2020. Short-term temperature forecasts using a convolutional neural network—An application to different weather stations in Germany. *Machine Learning with Applications*, 2: 100007.
- Kuligowski, R. J.; and Barros, A. P. 1998. Localized precipitation forecasts from a numerical weather prediction model using artificial neural networks. *Weather and forecasting*, 13(4): 1194–1204.
- Kumar, P.; Nema, M. K.; Thayyen, R. J.; Goel, M.; and Jain, S. K. 2013. Trend analysis of Hydrological variables in Western Himalayan region-Phase I (JAMMU & KASHMIR). Technical report, National Institute of Hydrology.
- Lai, G.; Chang, W.-C.; Yang, Y.; and Liu, H. 2018. Modeling long-and short-term temporal patterns with deep neural networks. In *The 41st international ACM SIGIR conference on research & development in information retrieval*, 95–104.
- Latake, P. T.; Pawar, P.; and Ranveer, A. C. 2015. The greenhouse effect and its impacts on environment. *Int. J. Innov. Res. Creat. Technol*, 1(3).
- Liu, P. J.; Saleh, M.; Pot, E.; Goodrich, B.; Sepassi, R.; Kaiser, L.; and Shazeer, N. 2018. Generating wikipedia by summarizing long sequences. *arXiv preprint arXiv:1801.10198*.
- Livieris, I. E.; Pintelas, E.; and Pintelas, P. 2020. A CNN–LSTM model for gold price time-series forecasting. *Neural computing and applications*, 32(23): 17351–17360.
- Lloyd, C. T.; Sturrock, H. J.; Leasure, D. R.; Jochem, W. C.; Lázár, A. N.; and Tatem, A. J. 2020. Using GIS and machine learning to classify residential status of urban buildings in low and middle income settings. *Remote Sensing*, 12(23): 3847.
- Ma, X.; Zhang, P.; Zhang, S.; Duan, N.; Hou, Y.; Zhou, M.; and Song, D. 2019. A tensorized transformer for language modeling. *Advances in neural information processing systems*, 32.
- Malczewski, J. 2004. GIS-based land-use suitability analysis: a critical overview. *Progress in planning*, 62(1): 3–65.
- Mandal, S.; Madhipatla, K. K.; Guttikunda, S.; Kloog, I.; Prabhakaran, D.; and Schwartz, J. D. 2020. Ensemble averaging based assessment of spatiotemporal variations in ambient PM_{2.5} concentrations over Delhi, India, during 2010–2016. *Atmospheric Environment*, 224: 117309.
- Mehrkanon, S. 2019. Deep shared representation learning for weather elements forecasting. *Knowledge-Based Systems*, 179: 120–128.
- Nguyen, T.; Tran, T.; Phung, D.; and Venkatesh, S. 2015. Tensor-variate restricted Boltzmann machines. In *Proceedings of the AAAI Conference on Artificial Intelligence*, volume 29.
- Ravuri, S.; Lenc, K.; Willson, M.; Kangin, D.; Lam, R.; Mirowski, P.; Fitzsimons, M.; Athanassiadou, M.; Kashem, S.; Madge, S.; et al. 2021. Skilful precipitation nowcasting using deep generative models of radar. *Nature*, 597(7878): 672–677.
- Salman, A. G.; Kanigoro, B.; and Heryadi, Y. 2015. Weather forecasting using deep learning techniques. In *2015 international conference on advanced computer science and information systems (ICACSIS)*, 281–285. Ieee.

- Shen, T.; Zhou, T.; Long, G.; Jiang, J.; and Zhang, C. 2018. Tensorized self-attention: Efficiently modeling pairwise and global dependencies together. *arXiv preprint arXiv:1805.00912*.
- Shi, X.; Chen, Z.; Wang, H.; Yeung, D.-Y.; Wong, W.-K.; and Woo, W.-c. 2015. Convolutional LSTM network: A machine learning approach for precipitation nowcasting. *Advances in neural information processing systems*, 28.
- Shih, S.-Y.; Sun, F.-K.; and Lee, H.-y. 2019. Temporal pattern attention for multivariate time series forecasting. *Machine Learning*, 108: 1421–1441.
- Soman, S. S.; Zareipour, H.; Malik, O.; and Mandal, P. 2010. A review of wind power and wind speed forecasting methods with different time horizons. In *North American power symposium 2010*, 1–8. IEEE.
- Trebing, K.; and Mehrkanoon, S. 2020. Wind speed prediction using multidimensional convolutional neural networks. In *2020 IEEE Symposium Series on Computational Intelligence (SSCI)*, 713–720. IEEE.
- Tucker, L. R. 1966. Some mathematical notes on three-mode factor analysis. *Psychometrika*, 31(3): 279–311.
- Vaswani, A.; Shazeer, N.; Parmar, N.; Uszkoreit, J.; Jones, L.; Gomez, A. N.; Kaiser, L.; and Polosukhin, I. 2017. Attention is all you need. *Advances in neural information processing systems*, 30.
- Weagle, C. L.; Snider, G.; Li, C.; van Donkelaar, A.; Philip, S.; Bissonnette, P.; Burke, J.; Jackson, J.; Latimer, R.; Stone, E.; et al. 2018. Global sources of fine particulate matter: interpretation of PM_{2.5} chemical composition observed by SPARTAN using a global chemical transport model. *Environmental science & technology*, 52(20): 11670–11681.
- Yang, J.; Li, C.; Dai, X.; and Gao, J. 2022. Focal modulation networks. *Advances in Neural Information Processing Systems*, 35: 4203–4217.
- Zaz, S. N.; and Romshoo, S. A. 2013. Recent variation in temperature trends in Kashmir Valley (India). *Journal of Himalayan Ecology & Sustainable Development*, 8: 42–63.
- Zhou, H.; Zhang, S.; Peng, J.; Zhang, S.; Li, J.; Xiong, H.; and Zhang, W. 2021. Informer: Beyond efficient transformer for long sequence time-series forecasting. In *Proceedings of the AAAI conference on artificial intelligence*, volume 35, 11106–11115.
- Zhu, X. X.; Tuia, D.; Mou, L.; Xia, G.-S.; Zhang, L.; Xu, F.; and Fraundorfer, F. 2017. Deep learning in remote sensing: A comprehensive review and list of resources. *IEEE Geoscience and Remote Sensing Magazine*, 5(4): 8–36.

Supplementary Material for "FATE: Focal-modulated Attention Encoder for temperature prediction"

Anonymous submission

Data Clustering

For the classification of construction data collected from the satellite images, we used four input variables, k-means clustering. K-Means clustering of features can be done based on location or attribute values. An unsupervised classification algorithm classifies features within a cluster so that entities with similar features are grouped in the same cluster.

The clustering is done to reduce the distance between the two objects or cluster centroid. The frequently used distance measure is quadratic or Euclidean distance. The pictorial clustering is given in Figure 1.

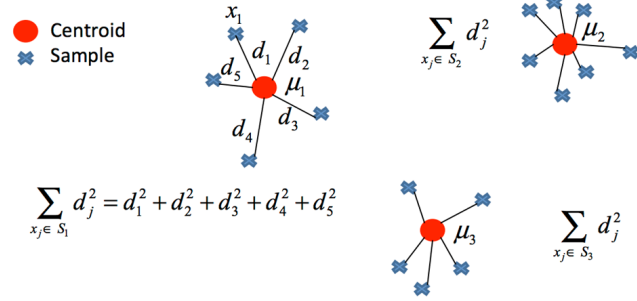


Figure 1: K-means Clustering

In this context, the rationale behind applying k-means clustering is to group similar features within a given dataset. Regarding construction data collected from satellite images, k-means clustering can group areas with similar construction patterns and characteristics, allowing for more accessible analysis and interpretation of the data. This approach is beneficial when dealing with large datasets, as it can help to identify patterns and trends that may not be immediately apparent to the human eye. Additionally, using unsupervised learning algorithms like k-means clustering can be helpful when the classes or categories within a dataset need to be more well-defined or known beforehand. In our proposed model, K-means is used to solve a classification and optimization problem by minimizing the function, which is the sum of the quadratic distances from each construction group to its cluster centroid.

All the objects in a group are represented by a d tensor: $x_1, x_2, x_3 \dots x_d$. We assume k groups with the sum of dis-

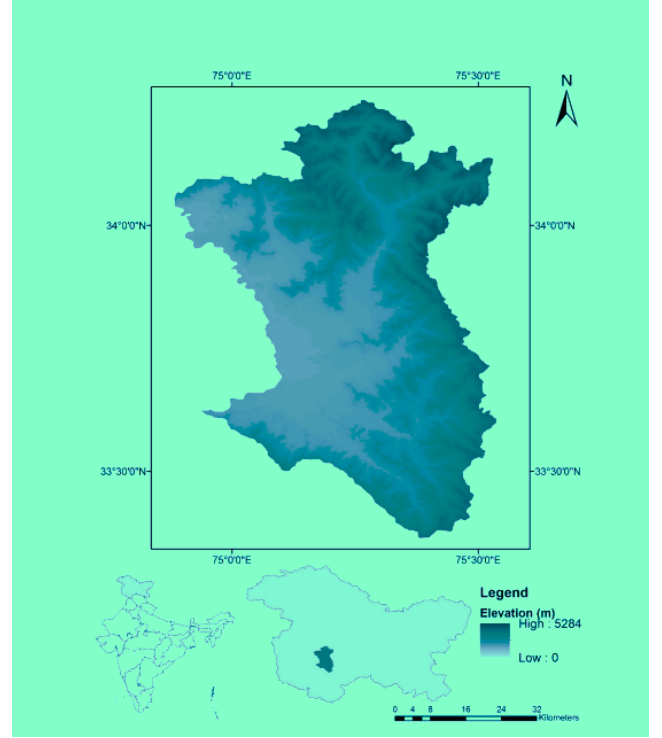


Figure 2: Data Collection: Region of Interest: This figure illustrates the process of data collection focused on a specific region of interest over a 39-year period.

tances of each Construction object to its centroid represented as $S = S_1, S_2, S_3 \dots S_k$. The equation to optimize is as follows:

$$\min_s E(\mu_i) = \sum_{x_j \in S_1} d_j^2 + \sum_{x_j \in S_2} d_j^2 + \sum_{x_j \in S_3} d_j^2 \quad (1)$$

Here S represents the entire construction dataset, and μ_i is the centroid of i^{th} group. We want to minimize the expected distance, and we have used the Gradient descent algorithm to achieve the same by doing a partial differentiation concerning the centroid as given in Equation 2.

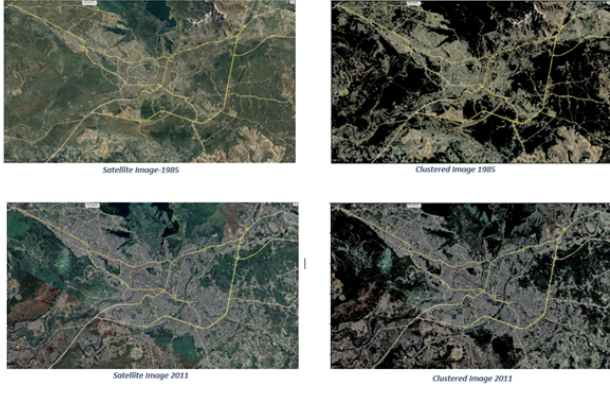


Figure 3: Construction Area Clusters over 39 Years. The figure illustrates the clustering results of construction areas across the region over a 39-year period, highlighting patterns and trends in urban development.

$$\frac{\partial E}{\partial \mu_i} = 0 \implies \mu_i^{t+1} = \frac{1}{|S_i^{(t)}|} \sum_{x_i \in S_i^{(t)}} x_i d \quad (2)$$

Figure 2 illustrates the *Region of Interest (ROI)* used in the data collection process. The ROI focuses on a specific area or feature within the dataset that is crucial for analysis. By defining this region, we ensure that the data collected is pertinent, enhancing the precision and relevance of the subsequent analysis.

Figure 4 displays a detailed view of the trends and variations in climate change parameters over time. The graph depicts fluctuations in these parameters across different years, revealing significant variations. These insights are essential for understanding the dynamic nature of climate change and for developing strategies to mitigate its effects.

Figure 4 shows the results of a K-means clustering analysis on satellite images of construction areas over a span of 39 years. This figure visualizes how construction areas have been clustered and evolved over time. It provides valuable insights into the spatial distribution and development patterns of infrastructure, highlighting changes and trends in urban expansion.

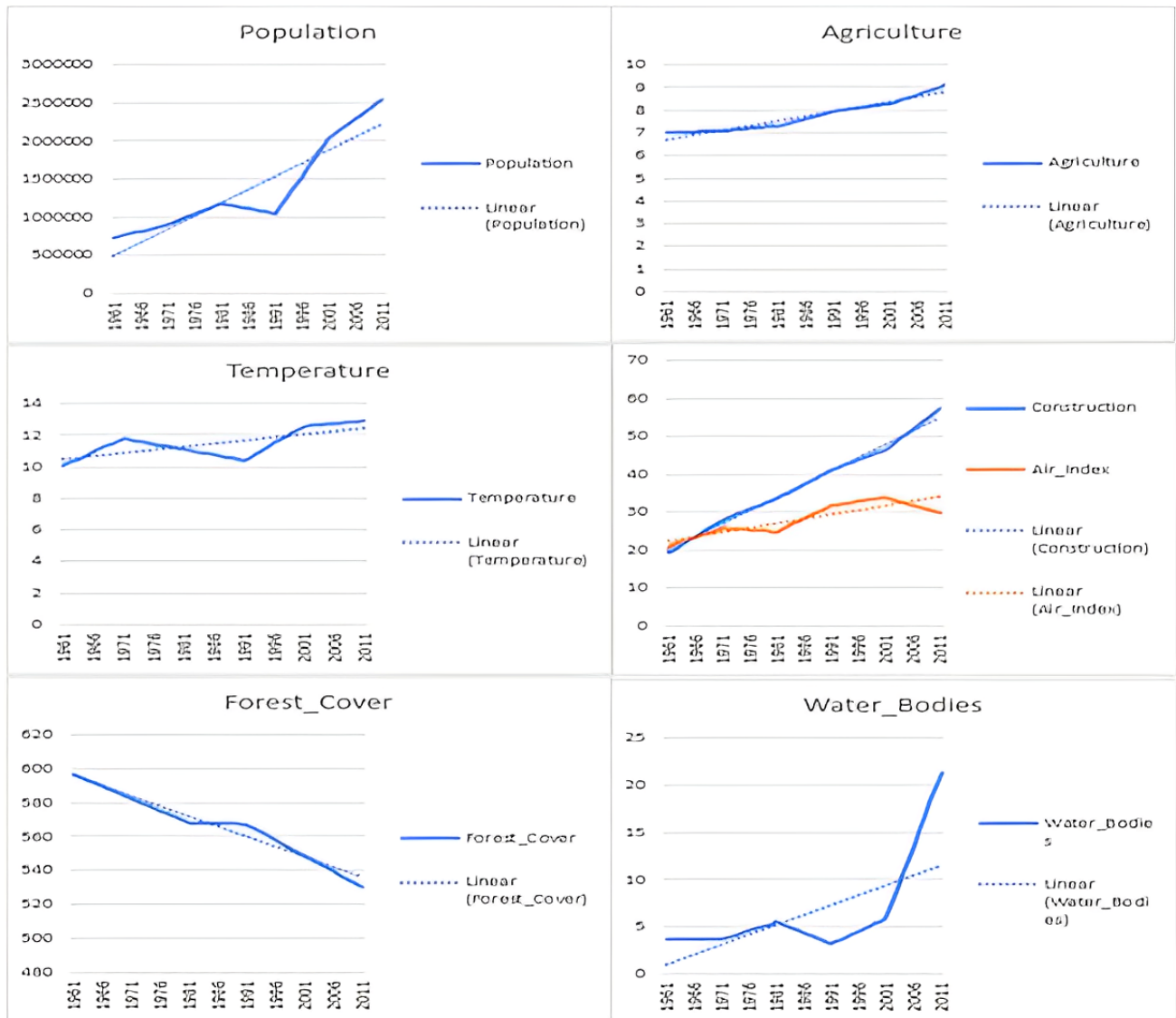


Figure 4: Exploring Trends and Variations in Climate Change Parameters: This figure presents the results of K-means clustering applied to construction area data over a 39-year period. The clusters represent different patterns and trends in urban development, reflecting variations in climate change parameters across the region. Each cluster highlights specific trends in construction activities, enabling a deeper understanding of how climate change has influenced urban growth and development over time. The analysis provides valuable insights into the correlation between climate change and urbanization, aiding in future urban planning and environmental impact assessments.